university of groningen / faculty of science and engineering

Gender Differences Between Anatomical Characteristics and Mechanical Properties of Porcine Urethra

Mihaela Daniela Culea
S4299906

Department of Biomedical Engineering UMCG
University of Groningen

Period: 21/04/2023 - 01/06/2023

Bachelor's Project

1st Examiner: Dr. P. Sharma, Associate Professor, Department of BiomedicalEngineering UMCG

2nd Examiner: Dr. Ir. J. Sjollema, Assistant Professor, Department of BiomedicalEngineering UMCG

Abstract

Urinary catheters, including the widely used Foley catheter, are essential for managing urine retention. However, they can lead to complications such as infections, primarily due to their design employing an inflated balloon. A promising solution consists of removing the balloon and engineering a coating that retains the catheter in place. This study investigates the urethra's anatomical characteristics and mechanical properties, intending to lay the groundwork for advanced catheter coatings. Extensive literature review and ex-vivo experiments using porcine urethra samples were conducted. Replicas of the urethral lumen were created using polydimethylsiloxane (PDMS) and analyzed through 3D scanning. This confirmed the irregular and non-circular nature of the luminal surface in the porcine urethra, as well as the anatomical structural distinctions between the two genders. Mechanical properties of different urethral sections were assessed using a Low Load Compression Testing (LLCT) machine, with a specific emphasis on stiffness and percentage of relaxation values. The mean stiffness remained consistent across all regions and between genders. Conversely, notable differences were observed in the relaxation percentage between the aforementioned independent variables. The primary aim of this research is to to provide a comprehensive understanding of the male and female porcine urethra. The expected outcome of this study is to contribute towards the development of safer and more effective urinary catheter designs, thereby minimizing complications and maximizing patient well-being.

Key words: urethra, lumen, urinary catheters, coating, anatomical characteristics, mechanical properties, Young's modulus, relaxation percentage.

Contents

1 Introduction **3**

2 Literature review **4**
2.1 The Urethra: a brief review 4
2.2 Background of urethral mechanical properties 7
2.2.1 Mechanical interactions during catheterization 7
2.2.2 Stiffness of biological tissue 9

3 Materials and methods **11**
3.1 Anatomical evaluation of the luminal space of the urethra 11
3.1.1 PDMS replicas 11
3.1.2 3D scans 12
3.2 Investigation of mechanical properties of the luminal space of the urethra . 13
3.2.1 Low Load Compression Testing 13
3.2.2 Statistical analysis 15

4 Results **17**
4.1 Anatomical evaluation of the urethral luminal space 17
4.2 Mechanical properties of the urethral lumen 17

5 Discussion **19**

6 Conclusion **21**

7 Bibliography **22**

1 Introduction

Urinary catheters have been widely utilized for centuries as essential medical devices for managing long-term urine retention, with the Foley catheter being one of the most commonly employed types (Zhu et al., 2018). The design of this indwelling catheter incorporates a balloon that is inflated post-insertion, effectively preventing the catheter from slipping out (Medline Plus, 2019). However, this arrangement often gives rise to well-known complications, including catheter-associated urinary tract infection (CAUTI), catheter-associated urethral injury (CAUI), catheter obstruction, and bladder mucosa irritation (Jeffery & Mundy, 2020). Among various potential solutions to mitigate these commonly encountered issues, include removal of the balloon and modification of the catheter surface with the use of a designed coating. (Majeed et al., 2019).

When developing such coatings, it is crucial to consider the properties and characteristics of both the biomaterial and the organs in direct contact with it. These coatings should possess anti-bacterial and anti-fouling properties to deter bacterial attachment and biofilm formation (Chadha et al., 2023). Additionally, they should effectively prevent catheter slippage without relying on a balloon mechanism.

This report presents a comprehensive analysis of the anatomical properties and mechanical characteristics of the urethra, based on extensive research and literature review. The study examines the forces between the urinary catheter and the urethral epithelial layer, as well as the stiffness of the biological tissue. Moreover, ex-vivo experimental research on male and female porcine urethra was conducted to supplement and compare the findings from the literature review, aiming to fill gaps in the understanding of the mechanical characteristics of the urethra. The ultimate objective of this study is to provide a comprehensive understanding of the male and female porcine urethra, which will serve as a foundation for future advancements in urinary catheter coatings. By bridging the knowledge gap regarding the urethra, this research aims to contribute to the development of safer and more effective catheter materials. Ultimately, these advancements will enhance patient care by reducing complications associated with long-term catheter use.

2 Literature review

2.1 The Urethra: a brief review

The urethra serves as the ultimate channel for the outflow of urine as the distal portion of the urinary system. In males, it performs a dual role by transporting not only urine but also semen. Its length stretches from the base of the urinary bladder to the external urethral opening (Marieb & Hoehn, 2019, p. 1036). Due to the anatomical variations between males and females, the male and female urethras exhibit distinct features.

In terms of its macroscopic anatomy, the most notable distinction is the size of the urethra. The male urethra measures approximately 18 cm to 20 cm in length and 8mm to 9mm in diameter, while the female urethra is only about 3 cm to 4 cm long and 6 mm in diameter (Abelson et al., 2018). Depending on the anatomical landmarks used, the male urethra can be classified into three segments: prostatic, membranous, and penile/spongy. The penile/spongy portion is further divided into three subdivisions, including the bulbous urethra, the pendulous urethra, and fossa navicularis (Reuter & Hikmat Al-Ahmadie, 2020). Identifying analogous landmarks on the female urethra is challenging, which makes precise classification difficult. However, the proximal portion can tentatively be defined as extending from the bladder to mid urethra, while the distal portion spans the area between the clitoris and vagina. Another distinguishing feature is the presence of paraurethral glands, such as the Skene glands in females and the Littre glands in males (Raspollini et al., 2019; Reuter & Hikmat Al-Ahmadie, 2020). Furthermore, the male urethra features a bulbourethral gland known as the Cowper's gland. Figure 1 and Figure 2 present visual illustrations depicting the anatomical division of the male and female urethra, respectively.

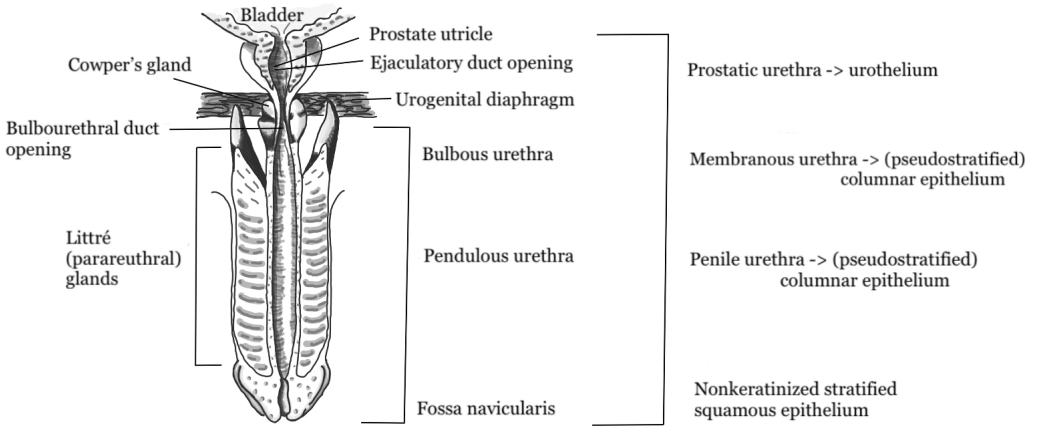

Figure 1: Schematic of male urethra anatomical division, together with the type of epithelium characteristic for each region

Microscopically, the lining of the urethra differs based on its position along the tube's length. In males, the urothelium typically lines the prostatic urethra, while the membranous portion and the majority of the penile urethra are lined with pseudostratified columnar epithelium. The fossa navicularis and the external urethral orifice, on the other hand, are usually lined with nonkeratinized stratified squamous epithelium. In females, the lining of

the urethra's proximal third is typically urothelium, which transitions to nonkeratinized stratified squamous epithelium distally (Reuter & Hikmat Al-Ahmadie, 2020).

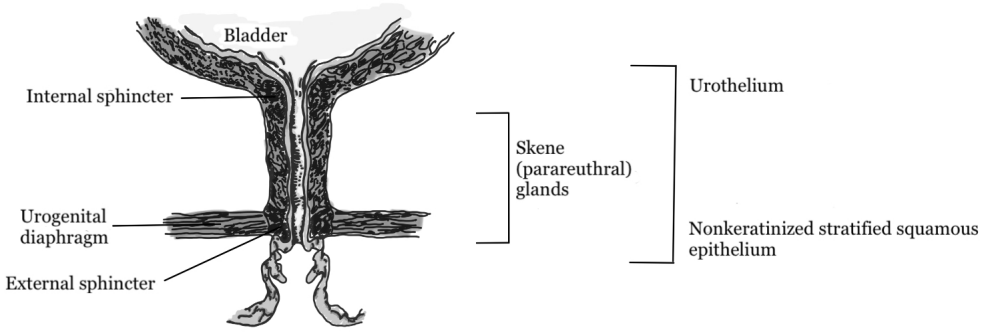

Figure 2: Schematic of female urethra anatomical division, together with the type of epithelium characteristic for each region

Based on the findings, it can be inferred that the urethral lining comprises three primary types of epithelium: urothelium, pseudostratified columnar epithelium, and nonkeratinized stratified squamous epithelium. Kierszenbaum et al. (2016) provides a comprehensive description of each epithelial type along with their respective characteristics. In humans, the urothelium is characterized as a pseudostratified epithelium. Notably, the urothelium exhibits a transitional configuration in response to the distension and contraction forces caused by urine, as described by Kierszenbaum et al. (2016). The pseudostratified epithelium is predominantly found in the epididymis, where it comprises two primary cell types: columnar cells and basal cells. The nonkeratinizing stratified squamous epithelium, also known as stratified squamous epithelium with moderate keratin, consists of distinct cell layers. Basal cells are specialized for mitotic division, while stratified cells cover the basal layer and undergo differentiation. Outer layer cells are highly differentiated and increase their keratin content, providing protection against the mechanical impact of urine on the tissue.

Additionally, a microscopic examination of the urethra's transverse section reveals the distinct and non-circular shape of the urinary fibromuscular tube. Pullan et al. (1982) conducted an extensive study to investigate the complex luminal shape of the urethra, one of its key characteristics. The objective of the study was to establish a relationship between the structure and function of the urethra. Various transverse sectional shapes of the urethra during relaxation and micturition were showcased, employing a radiological method. The findings emphasized the noticeable irregularities on the luminal side of the urethra, while also connecting them to the elasticity of the urethral wall. In their publication, Ishii et al. (2014) presented a methodology for constructing a three-dimensional model of the prostatic urethra using a cystourethroscope as a scanning tool. The panoramic images used in the model were obtained from clinical videos captured by a flexible video endoscope. This approach provided compelling visual evidence of the irregularities present on the luminal surface of the urethra, further confirming the observations made by Pullan et al. (1982).

The study's focus on the urethral lumen necessitates a cross-sectional view to provide a comprehensive depiction of the three primary layers encompassing it (inner to outer): epithelial, submucosal, and muscular. In males, the muscular layer consists mainly of smooth muscle cells, while the striated component forms the external urethral sphincter, which is responsible for active continence. The extracellular matrix (ECM) structure present in each cell layer is intricate and comprises collagen I and III, glycosaminoglycans (GAGs), and elastin (Abbas et al., 2019). The mechanical properties of elastic tissues rely on the collective presence of collagen and elastin as fibrous components. Collagen fibers provide strength and structural support to the tissue, while elastin plays a crucial role in conferring elasticity (Coenen et al., 2018). Apart from maintaining cellular homeostasis, the ECM is vital in determining urethra's mechanical elastance (reciprocal of compliance), enabling it to expand or stretch in response to changes in urethral pressure (Thind et al., 1991).

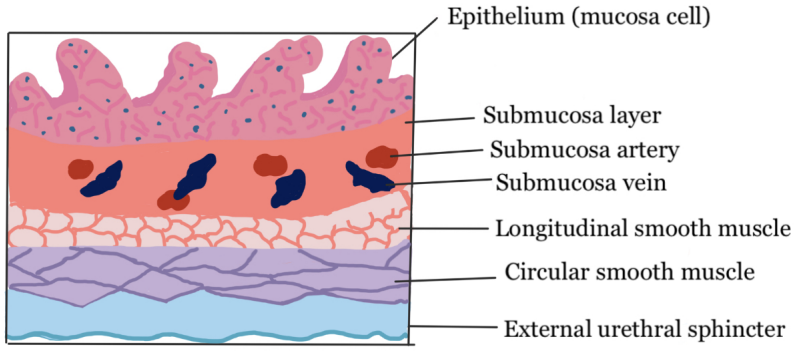

Figure 3: Schematic of transverse section of urethra containing the types of layers that comprise it; epithelium is present at the inner/luminal side of the urethra.

Within the female urethra, the muscular layer comprises both urethral smooth muscle and striated muscle. The former is composed of an inner and outer layer, with the inner layer consisting of lengthwise arranged smooth muscle fibers surrounding the urethral lumen, see Figure 3 (Mistry et al., 2019). This layer's elasticity results in the longitudinal smooth muscle bundle expanding, narrowing the urethral lumen and increasing urination resistance. The outer layer is made up of circular smooth muscle fibers that are fatigue-resistant and slow-contracting (Yang et al., 2023). The female urethral wall, like its male counterpart, is predominantly rich in proteins such as collagen and elastin. Additionally, the elasticity of the urethral wall plays a critical role in determining the flow resistance when the surface of the urethral lumen is covered with mucus. The greater the elasticity of the urethral wall, the higher the flow resistance will be (Zinner et al., 1983).

The submucosal layer of the urethra is rich in blood vessels that supply the mucous membrane with blood (Figure 4). This results in cell proliferation, thickening of the mucous membrane, increased mucus secretion and improved sealing performance of the urethral lumen (Mistry et al., 2019). Low estrogen levels can cause insufficient mucosal blood supply that will ultimately result in urinary incontinence (Yang et al., 2023).

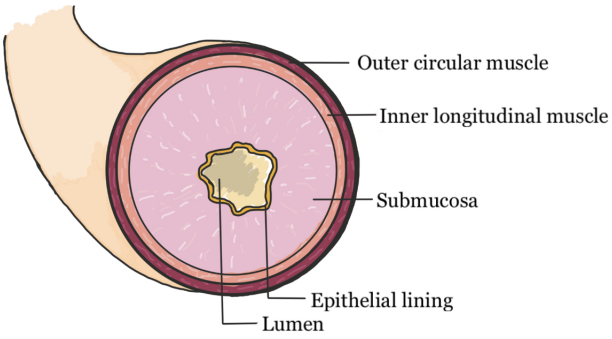

Figure 4: Schematic of cross-section of urethra

The urethral mucosa, which forms the innermost layer, serves as a sealing barrier for the urethral lumen. This function is assisted by the production of mucus-like secretions from the mucosa, which is supported by the submucosal blood vessels (Yang et al., 2023).

2.2 Background of urethral mechanical properties

The assessment of mechanical properties plays a crucial role in predicting how tissues will perform when subjected to different types of deformational forces, such as tensile, compression, flexural, and torsional forces (Shrivastava, 2018). This holds particularly true when it comes to the implantation or insertion of a urinary catheter. Cunnane et al. (2021) establishes a clear connection between the mechanical properties of the urethra and the specific composition of its tissue, highlighting the crucial role played by elastin and collagen fibers. Moreover, the study finds that this relationship mirrors that of other tubular soft biological tissues, such as arteries. Hence, it is imperative to possess a thorough comprehension of the mechanical characteristics of the urethral tissue when developing an efficient urinary catheter.
This section explores the key mechanical properties relevant for understanding the final outcomes of the experimental research. Primarily, this part provides a concise overview of the forces exerted on the urethra during the process of inserting a urinary catheter, as well as the forces acting on it after placement. Subsequently, the study emphasizes the significance of urethral tissue stiffness as a central focal point, while briefly introducing the concept of the stress relaxation modulus.

2.2.1 Mechanical interactions during catheterization

In the realm of urinary catheterization, the direct interaction between urinary catheters and the luminal surface of the urethra necessitates a comprehensive recognition and understanding of the forces at play. This understanding is crucial for the design of urinary catheters that are both efficient and appropriate. When examining the forces exerted on the urethra within the context of urinary catheterization, two specific scenarios warrant discussion. Firstly, the forces encountered during the insertion of the urinary catheter, and secondly, the forces experienced by the urethra once the catheter has been successfully placed.

No existing studies have been identified that address this specific issue. However, a relevant study conducted by Wagner et al. (2021) focuses on the tribological aspects and stenting process of blood vessels. In terms of force dynamics, the insertion of a urinary catheter along the urethra bears resemblance to the placement of a stent within a blood vessel. The interaction between the stent and the vessel layer shares similarities with the interaction between a urinary catheter and the urethral layer in the static state after catheterization. While the analysis of vessel catheter insertion is inherently dynamic, it can be regarded as comparable to the process of inserting a urinary catheter through the urethra during catheterization. Additionally, in a study conducted by Cunnane et al. (2021), it was discovered that the correlation between the composition of urethral tissue and its mechanical properties closely resembles that of other soft biological tissues with tubular structures, such as arteries. Therefore, the study by Wagner et al. (2021) can serve as a basis for comparing and analyzing these forces. Consequently, a comprehensive examination of the tribology involved in the process of catheterization is subsequently provided, with the aforementioned article serving as the primary source of information.

In the first scenario, when the urinary catheter is securely in place after catheterization, several key forces act upon the urethra, as revealed by the free body diagram in Figure 5. These forces include the normal force F_N, friction force F_F, and hemodynamic force F_H. The normal force F_N arises from the contact pressure between the urethral wall and the catheter tube. It is a contact force exerted by the urethral wall onto the catheter tube. The friction force F_F emerges as a consequence of the interaction between the normal force and the urine flow. It is influenced by the static friction coefficient μ_S and plays a critical role in maintaining the position of the catheter by counteracting the hemodynamic force F_H. The hemodynamic force F_H, on the other hand, is generated by the flow of urine. It is the driving force behind the urine flow and contributes to the overall forces acting on the urethra. It is important to note that the hemodynamic force is time-dependent as it varies with the duration of micturition.

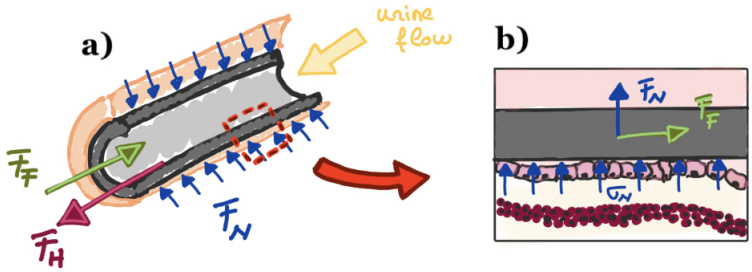

Figure 5: Schematic drawing of urinary catheter placed inside the urethra. a) Forces acting on the catheter. Between the lumen of the urethra and the catheter, normal force F_N gives rise to friction force F_F, which acts against the hemodynamic force F_H. b) Detailed view of the interaction between the catheter and the endothelial layer. Normal pressure σ_N of this interaction results in normal force F_N and friction force F_F.

The second scenario involves the insertion of a urinary catheter, which is a more intricate process. The schematic of this scenario can be visualized in Figure 6. During insertion,

the catheter moves at a certain speed v through the urethral passage. There are several forces at play in this situation. Firstly, there is a normal force F_N exerted at the contact area $A_{contact}$ between the catheter and the inner surface of the urethra, resulting from the pressure applied by the vessel wall. Consequently, friction force F_F is present. In addition to these forces, there is the manual force F_{Manual} exerted by the person performing the catheter insertion, which can be determined from the parallelogram formed by the normal and friction forces (Figure 6 b)). A closer look of the contact area between the catheter and luminal wall, displays the normal pressure σ_N between endothelial cells and catheter under tangential speed v_t(Figure 6 b)). One crucial factor that affects the friction force and, thus, the resistance experienced, is lubrication. Higher resistance in the urethra can potentially cause damage to the endothelium. Therefore, reducing resistance can minimize the risk of tissue damage. This can be achieved by lubricating or coating the medical device before insertion.Furthermore, the lumen naturally provides lubrication through the secretion of mucus by the submucosa. A better comprehension of the tribology (study of friction, lubrication, and wear) of the urethra can be attained by modeling the interaction between the catheter and the tissue at the contact area.

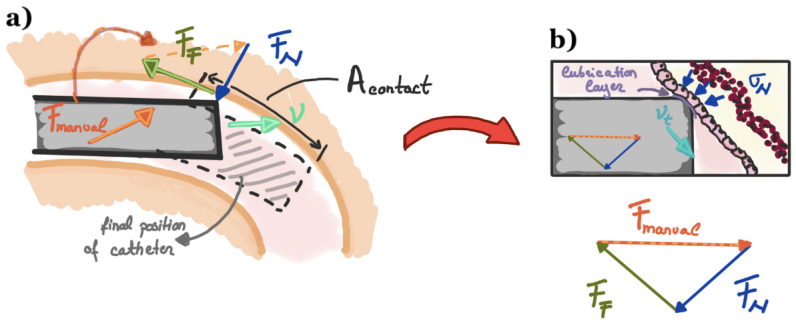

Figure 6: Schematic cross-section view of the catheterization process (during insertion). a) Catheter moving with speed v until initial contact. Further movement of catheter marked by dotted outline. Contact at contact area $A_{contact}$ causing friction. F_{manual} represents the insertion force applied during the process of catheterization, and it can be determined from the parellelogram of forces F_F and F_N. b) Detailed view of the interaction between the catheter and the endothelial layer with normal pressure σ_N under tangential speed v_t.

2.2.2 Stiffness of biological tissue

Stiffness, within the realm of biology, encompasses the mechanical properties of biological substrates (Handorf et al., 2015). It can be understood as the Elastic modulus, specifically Young's modulus, which characterizes the resistance to deformation (Wells, 2013). It serves as an indicator of whether a material is rigid (hard) or compliant (soft) (Handorf et al., 2015). Young's modulus is determined by dividing the magnitude of stress by the induced strain resulting from the stress. Figure 7 demonstrates the stress-strain curve, from which the slope of the elastic region is extracted to ascertain the Young's modulus of a particular material. A steeper slope indicates greater stiffness, while a shallower slope indicates lower stiffness. Stress refers to the force applied per unit area, while strain refers to the deformation, which

can manifest as normal (compression or tension) or shear. The concept of Young's elastic modulus E relates to a material's ability to resist compressive or elongating forces and is measured in units of Pascal (Pa) (Wells, 2013). When stress is applied up to the yield point, the material behaves elastically, signifying that it will return to its original form and size once stopped from appling the force. However, if the yield point is surpassed, the material undergoes permanent deformation after continuous stress (Thomas, n.d.).

When examining biological tissue, it is essential to consider its specific properties as they significantly influence the values of stress and strain. One such property is anisotropy, which stands in contrast to isotropy where uniformity exists in all directions. Anisotropy, on the other hand, is dependent on the direction of an applied force, thus introducing directional dependence (Tonndorf et al., 2021). Another important property of biological tissues is viscoelasticity, which indicates that they possess both viscous and elastic characteristics. Unlike perfect elasticity, viscoelastic tissues exhibit a degree of viscosity, implying that their deformation response to an applied force changes over time, resembling the behavior of liquids (Wells, 2013). According to Huang et al. (2012), various soft tissue types exhibit stiffness values ranging from 0.1 to 100kPa. This statement is assisted by a diagram illustrating the relative stiffness of different tissues, categorizing brain tissue as having the lowest stiffness value ($<$1kPa), while pre-calcified bone is depicted as having the highest stiffness value.
In general, tissues with higher stiffness or elastic modulus, such as cartilage or bone, display greater resistance to shape changes when subjected to physical forces. Conversely, softer tissues like fat tissue, bone marrow, or the brain exhibit the opposite behavior (Handorf et al., 2015).

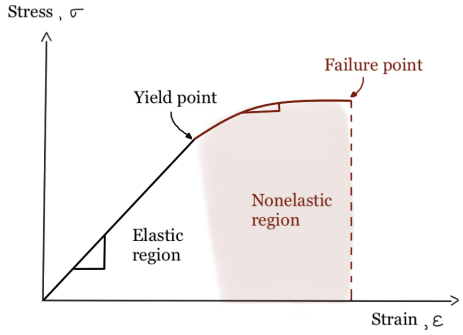

Figure 7: Example of a simple stress-strain curve. Young's modulus can be calculated by dividing the stress by the strain.

While stiffness pertains to the initial resistance exhibited by a material against deformation, stress relaxation characterizes the gradual relaxation of this resistance over time (Adebowale et al., 2021). The relaxation modulus, specific to viscoelastic materials, quantifies this behavior (Xu & Engquist, 2018). Additionally, substrate stress relaxation influences the type and extent of adhesions formed between cells and the substrate, with the precise relationship relying on the specific cell and substrate types involved (Adebowale et al., 2021).

3 Materials and methods

This section provides a comprehensive description of the two ex-vivo experiments conducted to address the study's research questions. The experiments were carried out under the supervision of professionals at the University Medical Center Groningen. Porcine biological samples, both male and female, obtained from the supplier 'Kroon Vlees' were utilized exclusively for all ex-vivo experiments.

The first experiment focused on examining the luminal structure of the urethra by replicating its nonuniformities using polydimethylsiloxane (PDMS). To analyze the resulting silicone impressions, comprehensive 3D scans were performed. This allowed for an easier visualization and future analysis of the luminal anatomy of the urethra. The second experiment aimed to determine the Young's modulus and relaxation time of three distinct cross-sections of the urethra using a Low Load Compression Testing (LLCT) machine. This measurement enabled the evaluation and comparison of the aforementioned mechanical properties along different regions of the urethra.

3.1 Anatomical evaluation of the luminal space of the urethra

The objective of this experiment was to evaluate the luminal structure of the porcine urethra by conducting a detailed analysis of silicone replicas created using PDMS. Through the utilization of PDMS, the experiment aims to closely examine the anatomy and characteristics of the urethral lumen. To perform the analysis, the silicone replicas obtained were subjected to 3D scanning at the University Medical Center Groningen. The results are presented in the form of the aforementioned modality, providing comprehensive insights into the observed findings.

To obtain a detailed walkthrough of the ex-vivo experiment, readers can refer to the protocol outlined in the Appendix A. This protocol provides a comprehensive, step-by-step explanation of the experimental procedure. By following the instructions provided, researchers can effectively replicate the experiment.

3.1.1 PDMS replicas

In this experiment, a total of six porcine urinary tracts were employed as biological samples, consisting of three male and three female specimens. Among these, two samples were freshly collected on the day of the experiment, while the remaining four were obtained several days prior. Upon collection, the bladder and underlying fat tissue were removed from all samples. The urethras were thoroughly cleaned and individually placed in separate cups containing phosphate-buffered saline (PBS) solution for preservation. The cups containing non-fresh samples were stored in a temperature-controlled room until they were utilized.

On the day of the experiment, the urethras were extracted from the preservation cups and carefully positioned on a tray situated on the laboratory table. For each biological sample, two distinct batches of silicone were prepared, with one batch stored in a cup and the other in a separate tupperware container. Due to the relatively quick solidification time of the

liquid silicone (approximately 20-30 minutes), both batches had to be prepared consecutively and in a timely manner. In the initial step, the duplicating silicone was prepared in a plastic cup with the intention of subsequent transfer into a syringe for injection into the lumen of the urethra. To create the duplicating silicone, equal amounts of Catalyst A and Base B solutions were mixed together. Specifically, 20 grams of each elastomer solution were weighed, combined in the cup, and meticulously blended with the use of a spoon to achieve a consistent and uniform distribution. Following this, the prepared silicone was allowed to rest for a brief duration, while the second batch of silicone was concurrently prepared in a plastic tupperware. In this instance, 80 grams of each elastomer solution were introduced into the container and mixed thoroughly before being set aside. Furthermore, the silicone prepared in the cup was carefully poured into a syringe, which was equipped with an additional plastic tip to facilitate the injection of the PDMS into the lumen of the urethra. After filling the syringe, the tip was cut to accommodate the experimental requirements, allowing the silicone to pass through smoothly. The syringe was cautiously inserted into one of the openings of the urethra, without introducing any silicone, until its tip nearly reached the adjacent opening. After ensuring the desired positioning of the syringe within the lumen, the PDMS solution was carefully injected. During the injection process, the syringe was gradually withdrawn to ensure complete filling of the interior of the urethra. Following this, the syringe was set aside and the urethra was immersed in the tupperware partially filled with silicone solution, guaranteeing complete coverage of the urethral surface. Subsequently, the tupperware was left undisturbed for approximately 30 minutes to enable solidification of the silicone.

Once the silicone had completely hardened, it was removed from the container. Using scissors, excess silicone was trimmed away to expose the section where the urethra was situated. This was easily done since the upper part of the urethra was still partially visible. Care was taken not to damage the tissue while extracting the silicone replica of the urethral lumen. Once detached, the replica was disinfected using an ethanol solution to ensure its suitability for future use. The same methodology was followed for each of the remaining biological samples. This procedure yielded a total of six silicone imprints, representing the luminal structure of both male and female porcine urethra.

3.1.2 3D scans

The silicone replicas underwent 3D scanning on 26 May 2023 at the Department of Dentistry and Oral Hygiene at UMCG. A '3Shape TRIOS 3' scanner, commonly used in the field of odontology, was employed for this purpose. To ensure effective scanning, it was necessary to keep the samples stationary while the scanning operator gradually moved along the length of the silicone replicas. To achieve this, the samples were securely attached to one end of a metal bar using glue and allowed to hang freely, as depicted in Figure 8. The top screw, passing through the bar, enabled movement of the samples in the frontal/coronal plane. Adjusting the distance between the bar and the surface on which the samples were positioned allowed the other end of the silicone replica to lightly touch the surface. This arrangement ensured that the samples remained immobilized during the scanning process.

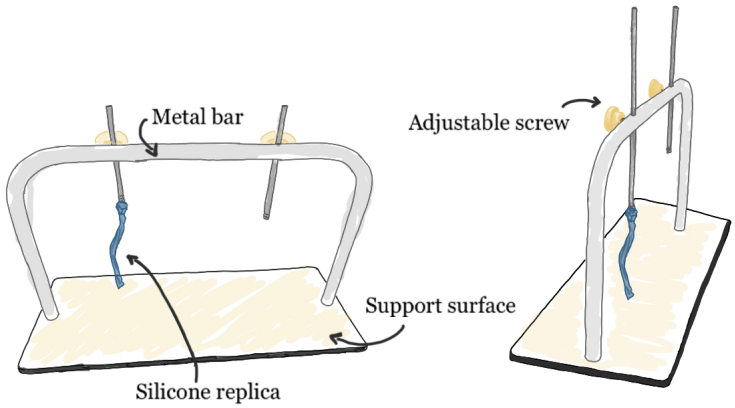

Figure 8: Setup for fixating the silicone replicas before 3D scanning.

The scanning process was initiated by activating the scanner and starting at one end of the sample, gradually moving along its length. Furthermore, the scanner was moved around the sample at a slow pace. This procedure resulted in the generation of a 3D scan of the sample, which was displayed on the connected computer and saved as an STL file. Each of the silicone replicas underwent the same process sequentially. To visualize the files, they were opened in the 3D viewer application. However, alternative application options are readily available as well. This enabled examination of the scanned object from various perspectives. In addition to rotational movements, the ability to zoom in was also accessible, providing detailed views of the scanned objects.

3.2 Investigation of mechanical properties of the luminal space of the urethra

The primary focus of this ex-vivo experiment was to investigate Young's modulus values of different segments within the urethra, as well as measure the percentage of relaxation time. These measurements were conducted using an LLCT machine. Following data processing, only the essential values were selected for further analysis. Considering the obtained final measurements, a two-way analysis of variance (ANOVA) test was conducted. The resulting values were then presented graphically to enhance comprehension and facilitate comparisons.

To obtain a detailed walkthrough of the ex-vivo experiment, readers can refer to the protocol outlined in the Appendix B. This protocol provides a comprehensive, step-by-step explanation of the experimental procedure. By following the instructions provided, researchers can effectively replicate the experiment.

3.2.1 Low Load Compression Testing

In order to ensure the integrity of the biological samples, fresh male and female porcine samples were collected each morning of the experiment. In total, six porcine urinary tracts were utilized, comprising three male and three female specimens. After collection, the urethras were meticulously separated from the urinary bladder, and any excess fat tissue

was subsequently removed.

To facilitate analysis, the samples were cut into smaller cross-sectional pieces, approximately 1 centimeter thick, to ensure compatibility with the LLCT machine. From each male and female sample, three cross-sections were chosen for further investigation. These cross-sections were specifically obtained from three distinct locations: near the external opening, in the middle of the urethra, and close to the bladder opening. To enhance the ease of analysis, the lumen of the urethra was given a more circular shape. This was achieved by inserting a plastic pipette tip into the lumen after carefully cutting it to reach the perfect size. This process aimed to open up the lumen without causing any stretching. Once this procedure was completed, the prepared sample was placed on a microscope slide and positioned inside the LLCT machine. Additionally, a suitable plunger was selected and attached to the LLCT. The plunger size was specifically chosen to be 1 millimeter, taking into account the thickness of the urethral wall cross-section.

The measurements were taken at three different regions within each cross section/biological replicate. Each region consisted of three sections defined as "superficial", "intermediate", and "deep", relative to their proximity to the lumen opening, providing a comprehensive analysis of the sample (Figure 9)).

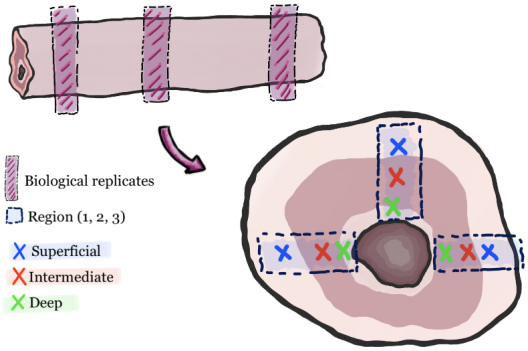

Figure 9: Schematic of section measurements at each region inside the cross-section of the porcine urethra samples.

Once the sample was positioned within the LLCT machine, the 'LLCT 2019 software' was accessed from the connected computer. The necessary parameters for analysis, such as sample type and plunger size, were selected, and the program was initiated. To begin, the support surface needed to be detected. The plunger was adjusted to be positioned above the microscope slide rather than the sample. The computer provided commands to modify the distance of the plunger from the surface, gradually approaching it as closely as possible without touching the glass. Once this adjustment was complete, the plunger automatically retracted upwards. For the subsequent step, the sample was placed beneath the plunger at the desired measurement point. The distance was again adjusted following the same procedure, ensuring proper alignment for analysis.

The waiting time for each measurement was displayed on the computer interface. Once the measurement was completed, saving the data was done by pressing 'Ok'. This process was repeated for each section within every region of the sample. It is important to note that localizing the support surface was necessary before every measurement. As a result, there were 9 measurements per biological replicate, totaling 27 measurements per urethra.

Following the practical phase of the experiment, data processing was carried out using the 'LLCT_Folder20022b Variable Plunger' program. The plunger size, in this case, was selected as 1 millimeter. The program converted the collected data into separate Excel sheets for each measurement, providing comprehensive data for further analysis and interpretation.

To streamline and condense the analysis of the final results, six customized tables were generated, corresponding to each urethra. These tables exclusively contained the pertinent data from each examined section that was crucial for achieving the experiment's objectives, such as relaxation percentage, stiffness values, tau, and relative importance. Furthermore, additional tables were created to present the average and standard deviation of the Young's modulus and of the relaxation percentage for each section of every biological replicate. This approach facilitated the plotting and comparison of values among the replicates, simplifying the analysis process. The final data utilized for additional statistical analysis is represented by these two tables (Appendix C).

3.2.2 Statistical analysis

After analyzing the data displayed in the two Excel tables, which include information on stiffness and relaxation percentage, the decision was made to conduct a two-way analysis of variance (ANOVA) test for each of the mechanical properties. As a consequence, this resulted in two individual two-way ANOVA tests that were performed separately using 'GraphPad Prism'.

The ANOVA test aims to assess the influence of two independent variables on a dependent variable (Hayes, 2021). Initially, the test was performed for stiffness. In this particular case, the independent variables are the regions of the urethra and the gender of the porcine samples, while the dependent variable is the stiffness of the urethra. The independent variable "regions" consists of three levels, namely superficial, intermediate, and deep, while the independent variable "gender" comprises two levels, male and female. Performing a two-way ANOVA allows for the assessment of the main effects of each independent variable (regions and gender), as well as the interaction effect between them. The main effects will determine if there are significant variations in stiffness between the regions and between male and female urethras. The interaction effect will indicate whether the influence of one variable depends on the levels of the other variable.

During the process of conducting a two-way ANOVA, three hypotheses need to be evaluated (MacKenzie, 2018). The initial two hypotheses aim to ascertain the influence of each factor on the response variable, while the third hypothesis investigates the presence of any interaction between the two factors. Thus, the three null hypotheses were set to be:

- H_0= The mean stiffness is the same across all regions (superficial, intermediate, and deep).
- H_0= The mean stiffness is the same for males and females.
- H_0= The effect of region on stiffness is the same for males and females (i.e., there is no interaction between region and gender).

Additionally, for the second mechanical property, the null hypotheses were set to be:

- H_0= The mean percentage of relaxation is the same across all regions (superficial, intermediate, and deep).
- H_0= The mean percentage of relaxation is the same for males and females.
- H_0= The effect of region on percentage of relaxation is the same for males and females (i.e., there is no interaction between region and gender).

The alternative hypotheses for each of these tests would suggest that there is a significant difference or interaction.

Finally, 'GraphPad Prism' was used to generate the final data required for interpretation. The first step involved transferring and organizing the Excel values into appropriate tables using a grouped table format. Subsequently, the significance level was set to 0.05. This corresponds to a 5% chance of type 1 error. In order to reject the null hypothesis, the p-value should be less than the significance level set. Consequently, this would mean that there is indeed a significant difference present. Running the program generated a table presenting specific data for the two-way ANOVA, including the percentage of total variation, the p-value, and the significance level. This was done for both, the stiffness and the percentage of relaxation. Lastly, the data was plotted as a confidence interval, which enabled the visualization of the mean values and margins of error for the two mechanical properties tested.

4 Results

4.1 Anatomical evaluation of the urethral luminal space

For the anatomical evaluation of the urethral luminal space, six biological samples were utilized, comprising three male and three female porcine urethras. As a result of the PDMS ex-vivo experiment, six replicated silicone models were generated, and all of them subsequently underwent 3D scanning. Figure10 and Figure 11 illustrate screenshots from a representative scan derived from a male porcine sample, showcasing the distinct features of the urethral anatomy. The upper portion of the scan corresponds to the external opening, while the lower section represents the connection point with the bladder. Upon closer examination (Figure 12), evident irregularities within the urethral lumen become apparent. This observation serves as clear evidence showcasing the distinctive attributes and non-circular nature of the luminal surface in the porcine urethra.

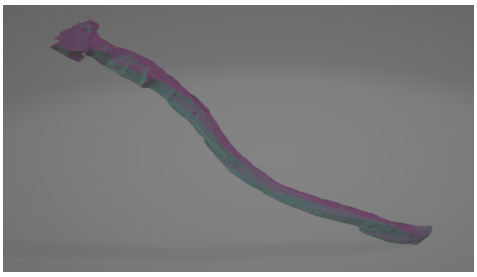

Figure 10: Screenshot from 3D scan performed on a silicone replica from a male porcine biological sample (one side view).

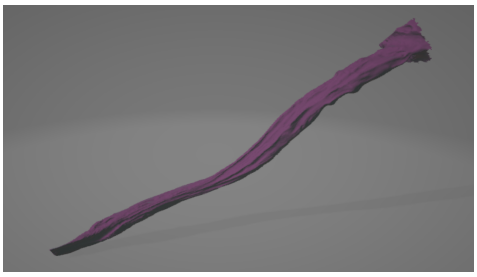

Figure 11: Screenshot from 3D scan performed on a silicone replica from a male porcine biological sample (one side view).

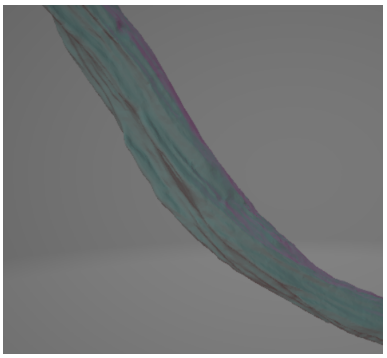

Figure 12: Screenshot from a zoomed in view of 3D performed on a silicone replica from a male porcine biological sample.

4.2 Mechanical properties of the urethral lumen

Two mechanical properties of the urethra were examined using LLCT measurements. The study included six biological samples of porcine urethras, and cross-sections were obtained from three distinct locations for further analysis. Within each cross-section, measurements

were taken at three different regions, consisting of three sections representing varying distances from the lumen. This resulted in a total of nine measurements per cross-section. The mean values and standard deviations were then tabulated in the final table (Appendix C). Subsequently, the statistical software 'GraphPad Prism' was utilized to conduct individual two-way ANOVA tests for each property. Firstly, the stiffness of the urethra was measured, and the resulting p-values are summarized in Table 1. For a visual representation, confidence intervals were plotted for each gender and urethra section, facilitating a clear visualization of the mean value and margin of error (see Figure 13). Following the same procedure, the relaxation percentage over a duration of 100 seconds was also analyzed, with the summary p-value provided in Table 2 and corresponding plots in Figure 14. For a comprehensive depiction of the ANOVA findings, readers are encouraged to refer to Appendix D. for detailed information.

Table 1: P-values for stiffness.

P value	Summary
0.8774	not significant
0.8480	not significant
0.1900	not significant

Table 2: P-values relaxation percentage.

P value	Summary
<0.0001	significant
<0.0001	significant
<0.0001	significant

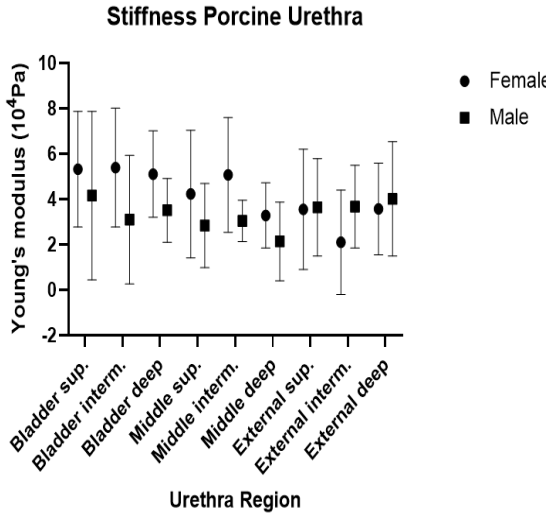

Figure 13: Confidence intervals of stiffness values for both genders at different urethral regions.

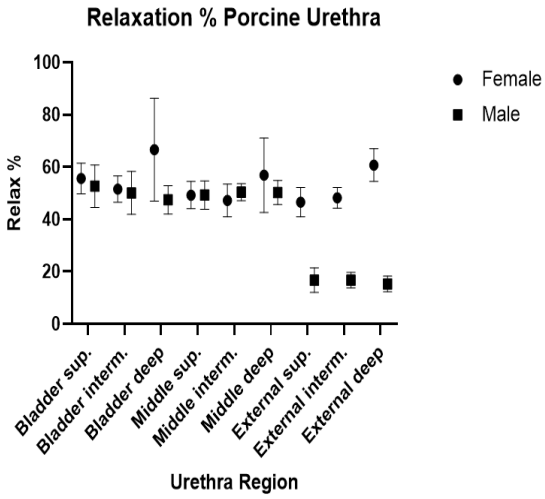

Figure 14: Confidence intervals of relaxation percentages for both genders at different urethral regions.

5 Discussion

The Discussion section serves as a critical component of this report, where the obtained results are carefully examined and analyzed. Through an in-depth exploration of the findings, this section aims to provide a comprehensive understanding of their implications and significance. By comparing and contrasting the results with existing literature and theoretical frameworks, we can gain valuable insights into the broader implications of the study. Additionally, this section will address any limitations or discrepancies encountered during the research process and propose potential directions for future investigations.

The initial research experiment aimed to address the main research question by examining and evaluating the luminal structure of both male and female porcine urethras. This was achieved by replicating the anatomical features of six biological samples using PDMS. Subsequently, the PDMS replicas were subjected to 3D scanning, allowing for detailed observation and assessment. The findings revealed several noteworthy observations regarding the urethral lumen. Upon closer scrutiny, it becomes evident that the urethral lumen exhibits noticeable irregularities. This finding serves as compelling evidence of the unique characteristics and non-circular morphology of the luminal surface in porcine urethras. Further observations were made regarding the dissimilarities between the male and female porcine samples. Specifically, it was observed that the male samples were significantly longer in comparison. Additionally, when examining transverse sections, notable distinctions were found in the thickness of the male urethra, which exhibited more muscle tissue compared to the female one. These findings validate the conclusions derived from the existing literature review. Moreover, the 3D scans possess the potential for alternative measurements, such as assessing the magnitude of deformations on the luminal surface of the urethra or conducting more in depth observations. For a more detailed examination of the urethra, other analytical methods could be implemented, especially if PDMS replication is not preferred. One suggestion is the utilization of a cystourethroscope, as previously mentioned and documented in the literature review section of the report. This approach would offer a closer and direct visualization of the urethra, enabling a more thorough assessment.

The second experimental research aimed to measure Young's modulus values in various segments of the urethra, together with the percentage of relaxation time. Similar to the first experiment, six biological samples of porcine urethra underwent testing, using an LLCT machine. The principal statistical analysis employed was a two-way ANOVA test. Firstly, the stiffness of the urethra was examined, where the null hypotheses failed to be rejected. This indicates that no significant differences were found in the stiffness values between genders and across different urethral regions. Surprisingly, this suggests that stiffness is mostly evenly distributed along the length of the urethra and does not vary significantly between genders, despite the male urethra having more muscle tissue. Regarding the findings for the second dependent variable, the relaxation percentage, the null hypothesis was rejected. This implies clear evidence of significant differences in relaxation percentage values between the two independent variables. The analysis of the plotted confidence intervals reveals a significant difference in values specifically observed in the external region of the male urethra. This region demonstrates a notably lower relaxation percentage over the 100-second time frame, with a small margin of error. This discrepancy could potentially be attributed to the tissue structure present in this region, specifically the fibroelastic connective tissue. However, it is

interesting to note that the external section of the female urethra exhibits a composition similar to that of the male urethra. Consequently, if the aforementioned hypothesis holds true, a larger discrepancy in the relaxation percentage of the female urethra in the external region would have been expected as well.

The observations made from the final results could potentially be influenced by certain limitations inherent in the study.One limitation of this study pertains to the relatively small sample size of six biological samples. Although efforts were made to ensure the reliability of the results, a larger sample size would have provided more robust and generalizable outcomes.

Furthermore, the non-uniform shape of the urethra posed challenges during measurements, particularly when assessing the mechanical properties at the three distinct regions. Positioning the plunger visually may have resulted in imprecise discrimination between these regions. In future research, employing a smaller plunger or employing alternative methods at a smaller scale could enhance the accuracy of measuring the mechanical properties. Consequently, a follow up limitation is the study solely relying on LLCT measurements and 3D scanning for analysis. Alternative methods or additional imaging techniques could provide complementary data to further enhance the accuracy and comprehensiveness of the results.

On top of that, the study was constrained by time limitations, which restricted the investigation to only measuring and analyzing the stiffness and relaxation percentage as mechanical properties. While these parameters offer valuable insights into urethral characteristics, they do not capture the entirety of urethral function. Future studies could explore additional mechanical properties or employ different measurement techniques to provide a more comprehensive understanding.

Another important limitation to consider, is the use of porcine urethras as biological samples. While they serve as a suitable model for studying urethral mechanics, it is crucial to recognize that there may be implicit anatomical and physiological differences between porcine and human urethras. Therefore, caution should be exercised when extrapolating these findings directly to human populations.

Lastly, it is important to acknowledge that this study was conducted under specific experimental conditions and limitations inherent to the chosen methodology. Factors such as sample preparation, measurement techniques, and statistical analyses may introduce their own sources of bias or error.

6 Conclusion

In conclusion, the study's findings indicate the presence of multiple deformations in the anatomy of the luminal surface of porcine urethras. Furthermore, the differences between male and female porcine samples were confirmed, particularly in terms of urethral length and thickness. Regarding the mechanical properties, no significant differences were observed in stiffness values. The mean stiffness remained consistent across all regions and between genders. However, contrasting results were obtained for the relaxation percentage, where significant differences were found between regions and genders. Having said that, it is crucial to acknowledge that these results are subject to certain limitations.
Nonetheless, it is important to focus on the limited literature review concerning the tribology of the urethra in order to address the need for further research. Exploring this field would yield valuable insights into the mechanical interaction between the catheter and the vulnerable organ (urethra), making it imperative to encourage progress in this specific area.

This conclusion was reached through a comprehensive research process that involved extensive literature review and two ex-vivo experiments conducted on porcine biological samples. Each experiment aimed to address a specific research question. The first experiment focused on examining the anatomical characteristics of the luminal surface of the urethra using PDMS replication and 3D scanning techniques.The second experiment aimed to investigate the stiffness and relaxation percentage values of the urethra, considering different cross-sections and distinct regions. These measurements were conducted using an LLCT machine, and data analysis involved two-way ANOVA testing.

Overall, this study offers a comprehensive understanding of the male and female porcine urethra, laying the groundwork for future advancements in urinary catheter coatings. The research strives to contribute to the development of safer and more efficient catheter coatings, with the ultimate goal of improving patient care by minimizing complications associated with long-term catheterization. By leveraging these findings as a foundation, future endeavors have the potential to advance the field and cultivate notable advancements in catheter technology.

7 Bibliography

Zhu, Z., Wang, Z., Li, S., & Yuan, X. (2018). Antimicrobial strategies for urinary catheters. Journal of Biomedical Materials Research Part A, 107(2), 445–467. https://doi.org/10.1002/jbm.a.36561

Medline Plus. (2019). Urinary catheters: MedlinePlus Medical Encyclopedia. Medlineplus.gov. https://medlineplus.gov/ency/article/003981.htm

Jeffery, N., & Mundy, A. (2020). Innovations in indwelling urethral catheterisation. BJU International. https://doi.org/10.1111/bju.14994

Majeed, A., Sagar, F., Latif, A., Hassan, H., Iftikhar, A., Darouiche, R. O., & Mohajer, M. A. (2019). Does antimicrobial coating and impregnation of urinary catheters prevent catheter-associated urinary tract infection? A review of clinical and preclinical studies. Expert Review of Medical Devices, 16(9), 809–820. https://doi.org/10.1080/17434440.2019.1661774

Chadha, J., Thakur, N., Chhibber, S., & Harjai, K. (2023). A comprehensive status update on modification of foley catheter to combat catheter-associated urinary tract infections and microbial biofilms. Critical Reviews in Microbiology, 1–28. https://doi.org/10.1080/1040841x.2023.2167593

Marieb, E. N., & Hoehn, K. (2019). Human anatomy & physiology (11th ed.). Pearson, 1006-1037.

Abelson, B., Sun, D., Que, L., Nebel, R. A., Baker, D., Popiel, P., Amundsen, C. L., Chai, T., Close, C., DiSanto, M., Fraser, M. O., Kielb, S. J., Kuchel, G., Mueller, E. R., Palmer, M. H., Parker-Autry, C., Wolfe, A. J., & Damaser, M. S. (2018). Sex differences in lower urinary tract biology and physiology. Biology of Sex Differences, 9. https://doi.org/10.1186/s13293-018-0204-8

Reuter, V. E., & Hikmat Al-Ahmadie. (2020). Urethra. Elsevier EBooks, 534-548.e5. https://doi.org/10.1016/b978-0-323-54941-7.00011-6

Raspollini, M. R., Cheng, L., Montironi, R., & Lopez-Beltran, A. (2019). Pathology of the Female and Male Urethra (A. Lopez-Beltran & M. R. Raspollini, Eds.). Cambridge University Press; Cambridge University Press. https://www.cambridge.org/core/books/ab/gynecologic-and-urologic-pathology/pathology-of-the-female-and-male-urethra/CD00B675D9E51B1709ED17FEDA86E358

Kierszenbaum, A. L., Tres, L. L., & Xiaopei Chen. (2016). Histology and Cell Biology: An Introduction to Pathology, Fourth Edition : an introduction to pathology. Elsevier.

Pullan, B., Phillips, J. I., & Hickey, D. S. (1982). Urethral Lumen Cross-Sectional Shape: Its Radiological Determination and Relationship to Function. 54(4), 399–407. https://doi.org/10.1111/j.1464-410x.1982.tb08953.x

Ishii, T., Yoichi Kambara, Tomonori Yamanishi, Naya, Y., & Igarashi, T. (2014). Urine Flow Dynamics Through Prostatic Urethra With Tubular Organ Modeling Using Endoscopic Imagery. IEEE Journal of Translational Engineering in Health and Medicine, 2, 1–9. https://doi.org/10.1109/jtehm.2014.2316148

Abbas, T. O., Yalcin, H. C., & Pennisi, C. P. (2019). From Acellular Matrices to Smart Polymers: Degradable Scaffolds that are Transforming the Shape of Urethral Tissue Engineering. International Journal of Molecular Sciences, 20(7), 1763. https://doi.org/10.3390/ijms20071763

Coenen, A. M. J., Bernaerts, K. V., Harings, J. A. W., Jockenhoevel, S., & Ghazanfari, S. (2018). Elastic materials for tissue engineering applications: Natural, synthetic, and hybrid polymers. Acta Biomaterialia, 79, 60–82. https://doi.org/10.1016/j.actbio.2018.08.027

Thind, P., Lose, G., & Colstrup, H. (1991). How to measure urethral elastance in a simple way. Urological Research, 19(4), 241–244. https://doi.org/10.1007/bf00305303

Mistry, M. A., Klarskov, N., DeLancey, J. O., & Lose, G. (2019). A structured review on the female urethral anatomy and innervation with an emphasis on the role of the urethral longitudinal smooth muscle. International Urogynecology Journal, 31(1), 63–71. https://doi.org/10.1007/s00192-019-04104-7

Yang, X., Wang, X., Gao, Z., Li, L., Lin, H., Wang, H., Zhou, H., Tian, D., Zhang, Q., & Shen, J. (2023). The Anatomical Pathogenesis of Stress Urinary Incontinence in Women. Medicina, 59(1), 5. https://doi.org/10.3390/medicina59010005

Zinner, N. R., Sterling, A. M., & Ritter, R. C. (1983). Evaluation of inner urethral softness Part II. Clinical study using new grooved probe device. Urology, 22(4), 446–448. https://doi.org/10.1016/0090-4295(83)90438-7

Shrivastava, A. (2018). Plastic Properties and Testing. Introduction to Plastics Engineering, 49–110. https://doi.org/10.1016/b978-0-323-39500-7.00003-4

Cunnane, E. M., Davis, N. F., Cunnane, C. V., Lorentz, K. L., Ryan, A., Hess, J., Weinbaum, J. S., Walsh, M., O'Brien, F. J., & Vorp, D. A. (2021). Mechanical, compositional and morphological characterisation of the human male urethra for the development of a biomimetic tissue engineered urethral scaffold. 269, 120651–120651. https://doi.org/10.1016/j.biomaterials.2021.120651

Wagner, R. M. F., Maiti, R., Carré, M. J., Perrault, C. M., Evans, P. C., & Lewis, R. (2021). Bio-tribology of Vascular Devices: A Review of Tissue/Device Friction Research. Biotribology, 25, 100169. https://doi.org/10.1016/j.biotri.2021.100169

Handorf, A. M., Zhou, Y., Halanski, M. A., & Li, W.-J. (2015). Tissue Stiffness Dictates Development, Homeostasis, and Disease Progression. Organogenesis, 11(1), 1–15. https://doi.org/10.1080/15476278.2015.1019687

Wells, R. G. (2013). Tissue Mechanics and Fibrosis. Biochimica et Biophysica Acta, 1832(7), 884–890. https://doi.org/10.1016/j.bbadis.2013.02.007

Thomas, S. (n.d.). How to Design for Stiffness Using Material Properties. Fictiv. Retrieved May 4, 2023, from https://www.fictiv.com/articles/how-to-design-for-stiffness-using-material-properties#: :text=It

Tonndorf, R., Aibibu, D., & Cherif, C. (2021). Isotropic and Anisotropic Scaffolds for Tissue Engineering: Collagen, Conventional, and Textile Fabrication Technologies and Properties. International Journal of Molecular Sciences, 22(17), 9561. https://doi.org/10.3390/ijms22179561

Huang, G., Wang, L., Wang, S., Han, Y., Wu, J., Zhang, Q., Xu, F., & Lu, T. J. (2012). Engineering three-dimensional cell mechanical microenvironment with hydrogels. Biofabrication, 4(4), 042001. https://doi.org/10.1088/1758-5082/4/4/042001

Adebowale, K., Gong, Z., Hou, J. C., Wisdom, K. M., Garbett, D., Lee, H., Nam, S., Meyer, T., Odde, D. J., Shenoy, V. B., & Chaudhuri, O. (2021). Enhanced substrate stress relaxation promotes filopodia-mediated cell migration. Nature Materials, 20(9), 1290–1299. https://doi.org/10.1038/s41563-021-00981-w

Xu, Q., & Engquist, B. (2018). A mathematical model for fitting and predicting relaxation modulus and simulating viscoelastic responses. Proceedings of the Royal Society A: Mathematical, Physical and Engineering Sciences, 474(2213), 20170540. https://doi.org/10.1098/rspa.2017.0540

Hayes, A. (2021, April 30). Two-Way ANOVA. Investopedia. https://www.investopedia.com/terms/t/two-way-anova.asp

MacKenzie, R. J. (2018, July 20). One-Way vs Two-Way ANOVA: Differences, Assumptions and Hypotheses. Informatics from Technology Networks; Technology Networks. https://www.technologynetworks.com/informatics/articles/one-way-vs-two-way-anova-definition-differences-assumptions-and-hypotheses-306553

Appendix

Appendix A

Protocol for analyzing the anatomy of the lumen of porcine urethra using duplicating silicone (PDMS)

The aim of this research is to assess the anatomy of the luminal space of the male and female porcine urethra using duplicating silicone to replicate the nonuniformities of the luminal side of the urethra.

Materials:

- Two porcine urinary tracts (one male and one female)
- PDMS/duplicating silicone solution (Catalyst A and Base B)
- Tweezers
- Scissors
- Scalpel
- Mixing spoon
- PBS solution
- Syringe
- Syringe tip
- Hard plastic tupperware
- Tray
- Weight

Methodology:

1. Collect the two porcine urinary tracts, one male and one female.
2. Separate the urethra from the urinary bladder and remove the underlying fat tissue from both samples.
3. If preserved overtime, place each of the urethras in separate cups containing PBS solution and deposit them in a cooler room.
4. Place the biological samples on a tray on the table.
5. Prepare two different batches of silicone, one in the cup, and one in the tupperware.

6. In a cup mix the two parts of the silicone elastomer (Catalyst A and Base B) on a 1:1 scale. To measure the quantities, place the cup on a weight and measure around 20 grams of Catalyst A and 20 grams of Base B.
7. Use a mixing spoon to combine the two solutions and set aside.
8. In a tupperware mix the two parts of the silicone elastomer (Catalyst A and Base B) on a 1:1 scale. To measure the quantities, place the tupperware on a weight and measure around 80 grams of Catalyst A and 80 grams of Base B.
9. Use a mixing spoon to combine the two solutions and set aside.
10. Take the silicone prepared in the cup and pour it into the syringe with the syringe tip attached to it.
11. When done pouring, use a cutting tool or scissors to cut the tip of the syringe.
12. Take one of the biological samples and inject its lumen with the liquid silicone solution.
13. Immediately after filling, place the biological sample in the tupperware full of liquid silicone.
14. Make sure the sample is covered and wait 30 minutes for the silicone to solidify.
15. After the silicone has hardened, take it out of the tupperware.
16. Carefully remove the extra silicone surrounding the urethra.
17. Take out the urethra and remove the silicone impression of the lumen (Figure 15).
18. Repeat steps 5-17 for the second biological sample as well.

Figure 15: Example of a final result after conducting the PDMS ex-vivo experiment; view of the silicone replica next to the biological sample used as reference.

Appendix B

Protocol for analyzing the Young's modulus and relaxation time of porcine urethra with the use of LLCT

The aim of this research is to assess the Young's modulus (stiffness) and relaxation time along different sections of the male and female porcine urethra using Low Load Compression Testing (LLCT).

Materials:

- Two porcine urinary tracts (one male and one female)
- LLCT machine (with 1mm plunger)
- Tweezers
- Scissors
- Scalpel
- Microscope slide
- PBS solution
- Plastic pipette tip

Methodology:

1. Collect the two porcine urinary tracts, one male and one female.
2. Separate the urethra from the urinary bladder and remove the underlying fat tissue from both samples.
3. Take one of the biological samples and cut a cross-section of approximately 0.5cm close to the external opening of the urethra.
4. Repeat step 3 two more times. Once for a cross-section from the middle of the urethra and once for a cross-section close to the bladder opening (Figure 17). Perform the measurements for each section as presented in Figure 16
5. Hydrate the cross-sections with PBS solution.
6. Take one plastic pipette tip and cut it to match the size of the cross-sectioned samples as much as possible.
7. Insert the pipette tip through the lumen of one of the cross-sections, with the end facing up.

8. Place the cross-section on a microscope slide and inside the LLCT machine (Figure 18).
9. Open LLCT2019 on the computer and adjust the settings to fit the tested material.
10. Find the glass surface: make sure the plunger is above the microscope slide and not the biological sample. Adjust the distance of the plunger from the surface until the plunger almost touches the microscope slide. Press 'OK'.
11. When the machine has found the glass surface, the plunger will go up by itself.
12. Move the biological sample below the plunger at the desired location, and again adjust the distance of the plunger until it almost touches the sample.
13. When done, the plunger will go up by itself.
14. Press 'OK' to save the data.
15. Repeat steps 10-14 for every location on the sample.
16. Repeat steps 6-14 for each cross-section.
17. Repeat steps 3-14 for the second biological sample (urethra) as well.
18. For data analysis: open LLCT F 1mm and select the file containing the data from the above experiment.
19. The programme will convert the information into an Excel file and save it automatically.

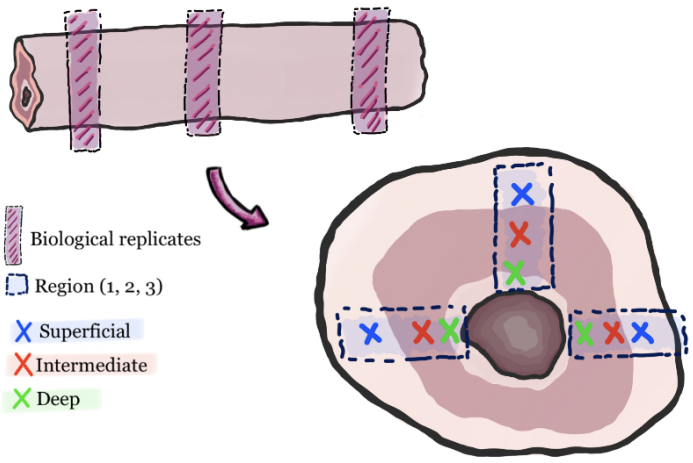

Figure 16: Schematic representation of section measurements at each region inside the cross-section of the urethra.

Figure 17: Example of biological replicates from the three distinct locations of the male urethra.

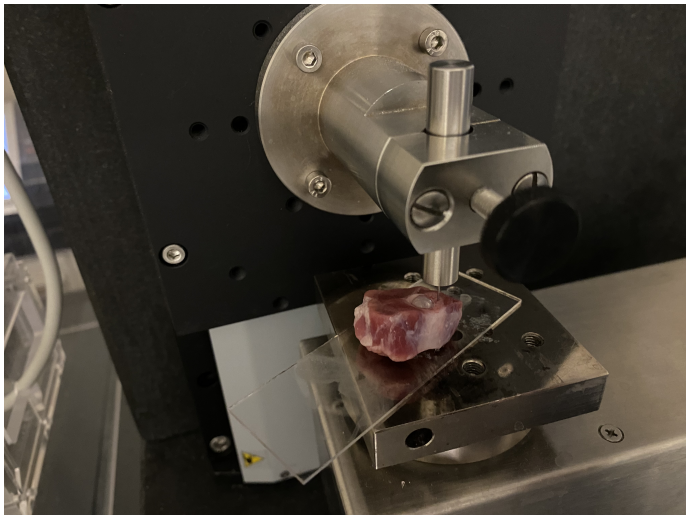

Figure 18: View of biological sample positioned into the LLCT machine before measurements.

Appendix C

Stiffness and relaxation percentage data used for the two-way ANOVA test

The two-way ANOVA test was performed in 'GraphPad Prism' making use of the mean values, standard deviation and number of samples for each independent variable (gender and region). The tables made use of the following data presented in Figure 19 for stiffness calculations, and in Figure 20 for relaxation percentage calculations.

Table format: Grouped		Group A Female			Group B Male		
		Mean	SD	N	Mean	SD	N
1	Bladder sup.	5.326667	2.548117	3	4.161111	3.71855968	3
2	Bladder interm.	5.395556	2.617857	3	3.103333	2.83436060	3
3	Bladder deep	5.108889	1.906997	3	3.513333	1.40450169	3
4	Middle sup.	4.231111	2.814580	3	2.841111	1.85440317	3
5	Middle interm.	5.075556	2.530845	3	3.046667	0.91219515	3
6	Middle deep	3.288889	1.431236	3	2.141111	1.73114445	3
7	External sup.	3.556667	2.651839	3	3.644444	2.15259791	3
8	External interm.	2.106667	2.298396	3	3.676667	1.81890077	3
9	External deep	3.574444	2.018775	3	4.013333	2.52229063	3

Figure 19: Screenshot from 'GraphPad Prism' with the data used to perform the two-way ANOVA statistical analysis for stiffness

Table format: Grouped		Group A Female			Group B Male		
		Mean	SD	N	Mean	SD	N
1	Bladder sup.	55.58667	5.906604	3	52.681111	8.12024083	3
2	Bladder interm	51.55556	5.015623	3	50.077778	8.23457464	3
3	Bladder deep	66.61444	19.662880	3	47.431111	5.46071068	3
4	Middle sup.	49.22444	5.198231	3	49.257778	5.47899575	3
5	Middle interm.	47.20889	6.260504	3	50.370000	3.26851266	3
6	Middle deep	56.83889	14.172690	3	50.243333	4.64127676	3
7	External sup.	46.56111	5.578519	3	16.745556	4.72715324	3
8	External interm	48.22889	3.903782	3	16.742222	2.94317195	3
9	External deep	60.74667	6.311097	3	15.288889	3.00538868	3

Figure 20: Screenshot from 'GraphPad Prism' with the data used to perform the two-way ANOVA statistical analysis for relaxation percentage

Appendix D

Stiffness and relaxation percentage ANOVA tables generated by 'GraphPad Prism'

The two-way ANOVA test was performed in 'GraphPad Prism' making use of the mean values, standard deviation and number of samples for each independent variable (gender and region). The two-way ANOVA tables generated as a result are presented as screenshots in Figure 21 and Figure 22.

	2way ANOVA					
1	Table Analyzed	Data 1				
2						
3	**Two-way ANOVA**	Ordinary				
4	Alpha	0.05				
5						
6	**Source of Variation**	**% of total variation**	**P value**	**P value summary**	**Significant?**	
7	Interaction	8.055	0.8774	ns	No	
8	Urethra section	8.802	0.8480	ns	No	
9	Gender	3.927	0.1900	ns	No	
10						
11	**ANOVA table**	**SS**	**DF**	**MS**	**F (DFn, DFd)**	**P value**
12	Interaction	19.35	8	2.419	F (8, 36) = 0.4576	P=0.8774
13	Urethra section	21.15	8	2.643	F (8, 36) = 0.5000	P=0.8480
14	Gender	9.433	1	9.433	F (1, 36) = 1.784	P=0.1900
15	Residual	190.3	36	5.286		
16						
17	**Difference between column means**					
18	Mean of Female	4.185				
19	Mean of Male	3.349				
20	Difference between means	0.8359				
21	SE of difference	0.6258				
22	95% CI of difference	-0.4332 to 2.105				
23						
24	**Data summary**					
25	Number of columns (Gender)	2				
26	Number of rows (Urethra section)	9				
27	Number of values	54				
28						

Figure 21: Screenshot from 'GraphPad Prism' with the data generated after performing the two-way ANOVA statistical analysis for stiffness

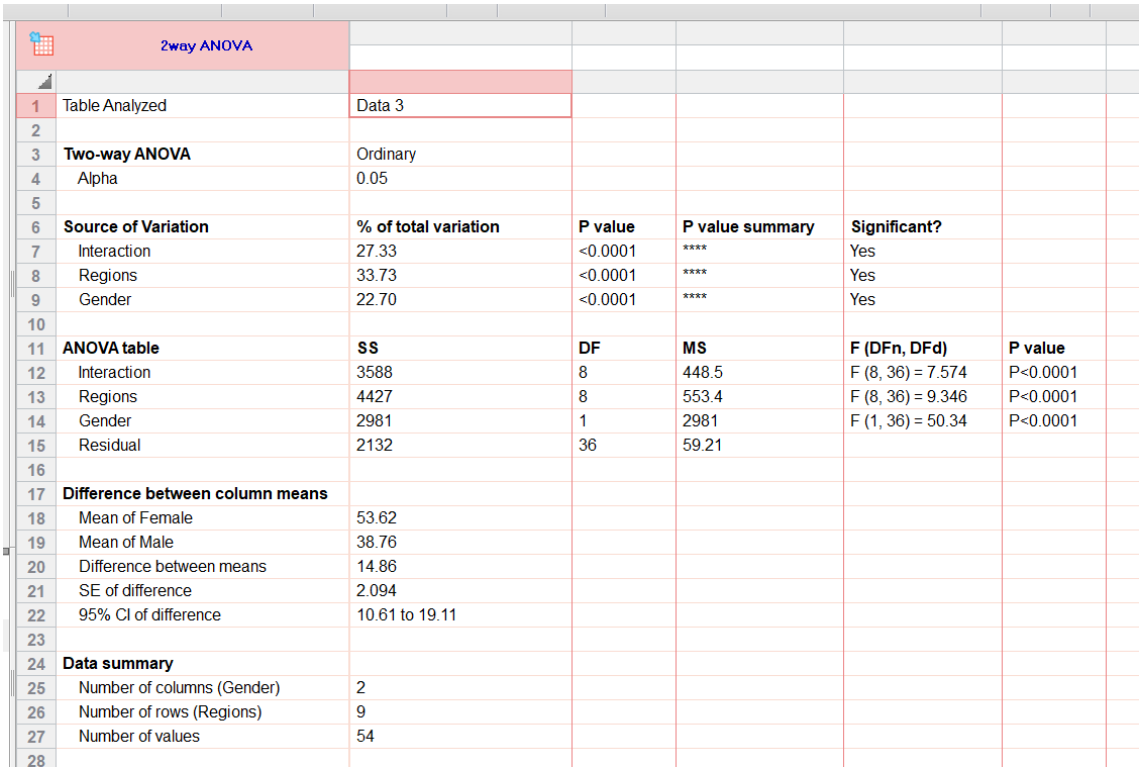

	2way ANOVA					
1	Table Analyzed	Data 3				
2						
3	**Two-way ANOVA**	Ordinary				
4	Alpha	0.05				
5						
6	**Source of Variation**	**% of total variation**	**P value**	**P value summary**	**Significant?**	
7	Interaction	27.33	<0.0001	****	Yes	
8	Regions	33.73	<0.0001	****	Yes	
9	Gender	22.70	<0.0001	****	Yes	
10						
11	**ANOVA table**	**SS**	**DF**	**MS**	**F (DFn, DFd)**	**P value**
12	Interaction	3588	8	448.5	F (8, 36) = 7.574	P<0.0001
13	Regions	4427	8	553.4	F (8, 36) = 9.346	P<0.0001
14	Gender	2981	1	2981	F (1, 36) = 50.34	P<0.0001
15	Residual	2132	36	59.21		
16						
17	**Difference between column means**					
18	Mean of Female	53.62				
19	Mean of Male	38.76				
20	Difference between means	14.86				
21	SE of difference	2.094				
22	95% CI of difference	10.61 to 19.11				
23						
24	**Data summary**					
25	Number of columns (Gender)	2				
26	Number of rows (Regions)	9				
27	Number of values	54				
28						

Figure 22: Screenshot from 'GraphPad Prism' with the data generated after performing the two-way ANOVA statistical analysis for relaxation percentage